Biophotonics and Biosensing

From Fundamental Research to Clinical Trials Through Advances of Signal and Image Processing

Photonic Materials and Applications Series

Published in association with the SPIE, the International Society for Optics and Photonics

Series Editor

Lorenzo Pavesi
University of Trento, Italy

Volumes in the series

Metal Halide Perovskites for Generation, Manipulation and Detection of Light
Edited by Juan P. Martínez-Pastor, Pablo Boix, Guichuan Xing

Metamaterials-by-Design
Edited by Andrea Alù, Nader Engheta, Andrea Massa, Giacomo Oliveri

Neuromorphic Photonic Devices and Applications
Edited by Min Gu, Elena Goi, Yangyundou Wang, Zhengfen Wan, Yibo Dong,
Yuchao Zhang, Haoyi Yu

*Biophotonics and Biosensing: From Fundamental Research to Clinical Trials Through
Advances of Signal and Image Processing*
Edited by Andrea Armani, Tatevik Chalyan, David D. Sampson

Photonic Materials and Applications Series

Biophotonics and Biosensing

From Fundamental Research to Clinical Trials Through Advances of Signal and Image Processing

Edited by

Andrea Armani
Department of Chemical Engineering and Materials Science
University of Southern California
Los Angeles, CA, United States

Tatevik Chalyan
Brussels Photonics (B-PHOT)
Department of Applied Physics and Photonics
Vrije Universiteit Brussel
Brussels, Belgium

David D. Sampson
School of Computer Science and Electronic Engineering
University of Surrey
Guildford, United Kingdom

ELSEVIER

Publisher's note: Elsevier takes a neutral position with respect to territorial disputes or jurisdictional claims in its published content, including in maps and institutional affiliations.

MATLAB® is a trademark of The MathWorks, Inc. and is used with permission.
The MathWorks does not warrant the accuracy of the text or exercises in this book.
This book's use or discussion of MATLAB® software or related products does not constitute endorsement or sponsorship by The MathWorks of a particular pedagogical approach or particular use of the MATLAB® software.

Notices

Knowledge and best practice in this field are constantly changing. As new research and experience broaden our understanding, changes in research methods, professional practices, or medical treatment may become necessary.

Practitioners and researchers must always rely on their own experience and knowledge in evaluating and using any information, methods, compounds, or experiments described herein. In using such information or methods they should be mindful of their own safety and the safety of others, including parties for whom they have a professional responsibility.

To the fullest extent of the law, neither the Publisher nor the authors, contributors, or editors, assume any liability for any injury and/or damage to persons or property as a matter of products liability, negligence or otherwise, or from any use or operation of any methods, products, instructions, or ideas contained in the material herein.

For information on all Elsevier publications
visit our website at https://www.elsevier.com/books-and-journals

"Hair follicle rainbow"
A skin organoid derived entirely from human pluripotent cells, containing hair follicles and a stratified epithelium.
Credit: Mattias Malaguti, Eleanor Earp and Maria Rosa Portero Migueles (Affiliation: The University of Edinburgh)

Working together
to grow libraries in
developing countries

www.elsevier.com • www.bookaid.org

Contents

List of contributors

Andrey Andreev

Division of Biology and Biological Engineering, California Institute of Technology, Pasadena, CA, United States

Brian E. Applegate

Caruso Department of Otolaryngology – Head & Neck Surgery, Keck School of Medicine, University of Southern California, Los Angeles, CA, United States

Department of Ophthalmology, Keck School of Medicine, University of Southern California, Los Angeles, CA, United States

Alfred E. Mann Department of Biomedical Engineering, Viterbi School of Engineering, University of Southern California, Los Angeles, CA, United States

Evgenia V. Azarova

Department of Materials Science and Engineering, Johns Hopkins University, Baltimore, MD, United States

Leonid Beliaev

DTU Electro – Department of Electrical and Photonics Engineering, Technical University of Denmark, Kongens Lyngby, Denmark

Thomas Bocklitz

Leibniz Institute of Photonic Technology, Member of Leibniz Health Technologies, Member of the Leibniz Centre for Photonics in Infection Research (LPI), Jena, Germany

Institute of Physical Chemistry (IPC) and Abbe Center of Photonics (ACP), Friedrich Schiller University Jena, Member of the Leibniz Centre for Photonics in Infection Research (LPI), Jena, Germany

Work group Artificial Intelligence in Spectroscopy and Microscopy, University of Bayreuth, Bayreuth, Germany

Anja Boisen

Technical University of Denmark, Department of Health Technology, Center for Intelligent Drug Delivery and Sensing Using Microcontainers and Nanomechanics, Kgs. Lyngby, Denmark

Michael R. Bryan

Department of Dermatology, University of Rochester, Rochester, NY, United States

Tatevik Chalyan

Brussels Photonics (B-PHOT), Department of Applied Physics and Photonics, Vrije Universiteit Brussel, Brussels, Belgium

Amey Chaware

Department of Biomedical Engineering, Duke University, Durham, NC, United States

M. Imran Cheema

Electrical Engineering Department, Syed Babar Ali School of Science and Engineering, Lahore University of Management Sciences (LUMS), Lahore, Pakistan

Dana Cialla-May

Leibniz Institute of Photonic Technology, Member of Leibniz Health Technologies, Member of the Leibniz Centre for Photonics in Infection Research (LPI), Jena, Germany

Institute of Physical Chemistry (IPC) and Abbe Center of Photonics (ACP), Friedrich Schiller University Jena, Member of the Leibniz Centre for Photonics in Infection Research (LPI), Jena, Germany

Jhonatan Contreras

Leibniz Institute of Photonic Technology, Member of Leibniz Health Technologies, Member of the Leibniz Centre for Photonics in Infection Research (LPI), Jena, Germany

Institute of Physical Chemistry (IPC) and Abbe Center of Photonics (ACP), Friedrich Schiller University Jena, Member of the Leibniz Centre for Photonics in Infection Research (LPI), Jena, Germany

Clare B. Cook

Department of Biomedical Engineering, Duke University, Durham, NC, United States

Pegah Dehbozorgi

Leibniz Institute of Photonic Technology, Member of Leibniz Health Technologies, Member of the Leibniz Centre for Photonics in Infection Research (LPI), Jena, Germany

Institute of Physical Chemistry (IPC) and Abbe Center of Photonics (ACP), Friedrich Schiller University Jena, Member of the Leibniz Centre for Photonics in Infection Research (LPI), Jena, Germany

Jeremy Delahanty

Department of Neuroscience, Johns Hopkins University School of Medicine, Baltimore, MD, United States

Stamatia Giannarou

Hamlyn Centre for Robotic Surgery, Department of Surgery and Cancer, Imperial College London, London, United Kingdom

Chhavi Goenka

Franklin W Olin College of Engineering, Needham, MA, United States

Roarke Horstmeyer

Department of Biomedical Engineering, Duke University, Durham, NC, United States
Department of Electrical and Computer Engineering, Duke University, Durham, NC, United States

Faiza Iftikhar

Electrical Engineering Department, Lahore College for Women University, Lahore, Pakistan

Oleksii Ilchenko

Technical University of Denmark, Department of Health Technology, Center for Intelligent Drug Delivery and Sensing Using Microcontainers and Nanomechanics, Kgs. Lyngby, Denmark
Lightnovo ApS, Birkerød, Denmark

Lucas Kreiss

Department of Biomedical Engineering, Duke University, Durham, NC, United States
Institute of Medical Biotechnology, Friedrich-Alexander University (FAU), Erlangen, Germany

Andrii Kutsyk

Lightnovo ApS, Birkerød, Denmark
Department of Energy Conversion and Storage, Technical University of Denmark, Kgs. Lyngby, Denmark
Faculty of Radiophysics, Electronics and Computer Systems, Taras Shevchenko National University of Kyiv, Kyiv, Ukraine

Andrei Laurynenka

DTU Electro – Department of Electrical and Photonics Engineering, Technical University of Denmark, Kongens Lyngby, Denmark

Ruihao Luo

Leibniz Institute of Photonic Technology, Member of Leibniz Health Technologies, Member of the Leibniz Centre for Photonics in Infection Research (LPI), Jena, Germany

Institute of Physical Chemistry (IPC) and Abbe Center of Photonics (ACP), Friedrich Schiller University Jena, Member of the Leibniz Centre for Photonics in Infection Research (LPI), Jena, Germany

Regina Magalhães

Caruso Department of Otolaryngology – Head & Neck Surgery, Keck School of Medicine, University of Southern California, Los Angeles, CA, United States

Benjamin L. Miller

Department of Dermatology, University of Rochester, Rochester, NY, United States

Azadeh Mokari

Leibniz Institute of Photonic Technology, Member of Leibniz Health Technologies, Member of the Leibniz Centre for Photonics in Infection Research (LPI), Jena, Germany

Institute of Physical Chemistry (IPC) and Abbe Center of Photonics (ACP), Friedrich Schiller University Jena, Member of the Leibniz Centre for Photonics in Infection Research (LPI), Jena, Germany

Sara Mostafapour

Leibniz Institute of Photonic Technology, Member of Leibniz Health Technologies, Member of the Leibniz Centre for Photonics in Infection Research (LPI), Jena, Germany

Institute of Physical Chemistry (IPC) and Abbe Center of Photonics (ACP), Friedrich Schiller University Jena, Member of the Leibniz Centre for Photonics in Infection Research (LPI), Jena, Germany

Kartikeya Murari

University of Calgary, Calgary, AB, Canada

Heidi Ottevaere

Brussels Photonics (B-PHOT), Department of Applied Physics and Photonics, Vrije Universiteit Brussel, Brussels, Belgium

Laura Pasquardini

Indivenire srl, Trento, Italy

Radhika K. Poduval

Massachusetts General Hospital, Boston, MA, United States

Harvard Medical School, Boston, MA, United States

Jürgen Popp

Leibniz Institute of Photonic Technology, Member of Leibniz Health Technologies, Member of the Leibniz Centre for Photonics in Infection Research (LPI), Jena, Germany

Institute of Physical Chemistry (IPC) and Abbe Center of Photonics (ACP), Friedrich Schiller University Jena, Member of the Leibniz Centre for Photonics in Infection Research (LPI), Jena, Germany

Diego Razura

Caruso Department of Otolaryngology – Head & Neck Surgery, Keck School of Medicine, University of Southern California, Los Angeles, CA, United States

James H. Quillen College of Medicine, Eastern Tennessee University, Johnson City, TN, United States

Alfie Roddan

Hamlyn Centre for Robotic Surgery, Department of Surgery and Cancer, Imperial College London, London, United Kingdom

Oleg Ryabchykov

Leibniz Institute of Photonic Technology, Member of Leibniz Health Technologies, Member of the Leibniz Centre for Photonics in Infection Research (LPI), Jena, Germany

Institute of Physical Chemistry (IPC) and Abbe Center of Photonics (ACP), Friedrich Schiller University Jena, Member of the Leibniz Centre for Photonics in Infection Research (LPI), Jena, Germany

Danuta M. Sampson

Lions Eye Institute, Nedlands, WA, Australia

The University of Western Australia, The School of Allied Health, Optometry Division, Perth, WA, Australia

David D. Sampson

School of Computer Science and Electronic Engineering, The University of Surrey, Guildford, United Kingdom

Anja Silge

Leibniz Institute of Photonic Technology, Member of Leibniz Health Technologies, Member of the Leibniz Centre for Photonics in Infection Research (LPI), Jena, Germany

Institute of Physical Chemistry (IPC) and Abbe Center of Photonics (ACP), Friedrich Schiller University Jena, Member of the Leibniz Centre for Photonics in Infection Research (LPI), Jena, Germany

Daniel J. Steiner

Department of Dermatology, University of Rochester, Rochester, NY, United States

Osamu Takayama

DTU Electro – Department of Electrical and Photonics Engineering, Technical University of Denmark, Kongens Lyngby, Denmark

Jack C. Tang

Caruso Department of Otolaryngology – Head & Neck Surgery, Keck School of Medicine, University of Southern California, Los Angeles, CA, United States

Clayton Walker

Caruso Department of Otolaryngology – Head & Neck Surgery, Keck School of Medicine, University of Southern California, Los Angeles, CA, United States

Department of Biomedical Engineering, Texas A&M University, College Station, TX, United States

Anna Wisniowiecki

Caruso Department of Otolaryngology – Head & Neck Surgery, Keck School of Medicine, University of Southern California, Los Angeles, CA, United States

Department of Biomedical Engineering, Texas A&M University, College Station, TX, United States

Chi Xu

Hamlyn Centre for Robotic Surgery, Department of Surgery and Cancer, Imperial College London, London, United Kingdom

Shiqi Xu

Department of Biomedical Engineering, Duke University, Durham, NC, United States

Linhui Yu

Massachusetts General Hospital, Boston, MA, United States

Harvard Medical School, Boston, MA, United States

Zhongyang Zhang

Technical University of Denmark, Department of Health Technology, Center for Intelligent Drug Delivery and Sensing Using Microcontainers and Nanomechanics, Kgs. Lyngby, Denmark

Kevin C. Zhou

Department of Biomedical Engineering, Duke University, Durham, NC, United States

Department of Electrical Engineering & Computer Sciences, University of California, Berkeley, CA, United States

Tissue optics

1

Chhavi Goenka[a] and Linhui Yu[b,c]

[a]Franklin W Olin College of Engineering, Needham, MA, United States, [b]Massachusetts General Hospital, Boston, MA, United States, [c]Harvard Medical School, Boston, MA, United States

1.1   Introduction

Tissue optics delves into light's interaction with tissue, encompassing the propagation of light within the tissue and the reciprocal modifications that arise between light and tissue.

Tissue is a collection of cells that perform the same function, often characterized by similar structures. Tissues can be categorized into different groups based on their morphology. For instance, epithelial tissues envelop the surfaces of organs, tracts, and skin, whereas the connective tissue group includes bones, cartilage, and blood. Muscle tissues, formed by muscle cells, reside within the inner linings of organs and skeletal structures. Neural tissue, comprising cellular clusters forming the nervous system, is another distinct category. Furthermore, tissues are often classified based on their structural attributes. These varied tissue classifications are significant, as they impact the manner in which light interacts with them due to variations in their structure and composition.

Light-tissue interactions are fundamental to understanding and working with biomedical optics. The turbidity and heterogeneity of biological tissues impact their interactions with light. Light carries energy and can impact biological tissues, depending on the wavelength of light used. In biomedical optics, the impacts of light and tissues on each other are exploited for the diagnosis and treatment of diseases and other physiological conditions.

Therapeutic methods use the changes light can make to tissue. Some examples are photodynamic therapy, dermatological treatments, and optogenetics. Imaging and diagnostics use the changes that light undergoes when interacting with biological tissues. Some examples of these include microscopy, pulse oximetry, and functional near infrared spectroscopy (fNIRS) for brain studies. All the interactions mentioned here can be used both for spectroscopic and imaging applications.

In this chapter, we are giving an overview of light-tissue interactions and the various processes those interactions involve. We will also discuss the optical properties of tissue and briefly describe the advantages of using light-tissue interactions for biomedical applications.

1.2   Optical properties of tissue

Optical properties of tissues determine how light interacts with them, determining how a diagnostic or therapeutic application will be achieved. These properties are critical

to the design of light-based medical devices. Some terminologies that are used to describe the optical properties of tissues are absorption coefficient, scattering coefficient, scattering anisotropy, and refractive index. The scattering and absorption coefficients together form the attenuation coefficient, which is also used to characterize biological tissues and determine light transport through the tissue. These are described in more detail in the next section, "Light-tissue interactions."

Various methods are used to accurately determine the optical properties of tissues. These methods can be categorized into two main types: indirect methods and direct methods. As the name suggests, direct methods are not model-dependent but use measurements of unscattered transmission and fluence rate. Both these measurements are not easy to implement. In the former, the primary challenge is the separation of scattered light from unscattered light. In the latter, detector position can introduce errors in the measurements (detectors too close to boundaries and sources can introduce measurement errors) [1]. Indirect methods are model-dependent and employ relationships between optical properties of the tissue and light-tissue interactions, such as absorption and scattering. Indirect methods can be of two types: noniterative and iterative. Noniterative methods employ measurements of diffuse reflection and transmission and determine scattering and absorbing coefficients from those measurements. Sometimes, other measurements, such as time-of-flight and photoacoustic effects, are also used as noniterative methods. Iterative direct methods include the very commonly used Monte-Carlo modeling [2] [3] [4]. These methods also use measurements of transmission, reflection, absorbance, scattering, but the use of iterative methods gives them the advantage of error correction, which other methods do not readily have. In this chapter, we will limit ourselves to the discussion of the Monte-Carlo method and describe it in more detail in Section 1.4.

1.3   Light-tissue interactions

The interaction between light and tissues depends on the optical properties of tissues, which were discussed in the previous section, and is also related to the properties of the light that is being used, i.e., wavelength, direction, intensity, etc. For example, near-infrared wavelengths have a higher penetration depth in human tissue, whereas ultraviolet wavelengths are more common in fluorescence excitation.

Fig. 1.1 highlights the basic effects of light-tissue interactions: (A) shows the effects at the air-tissue interface: refraction and specular reflection, and (B) shows the effects when light propagates through tissue: light scattering and absorption, and the resulting diffuse reflectance and transmission.

1.3.1   Refraction

The change in direction of light propagation as it travels from one medium to another is called refraction. Refraction depends on the refractive indices of the two media. Refractive index (RI) is defined as the speed of light in a vacuum divided by the speed of light in the medium through which light is traveling. In diagnoses, refractive indices can be used for various applications such as differentiating between malignant
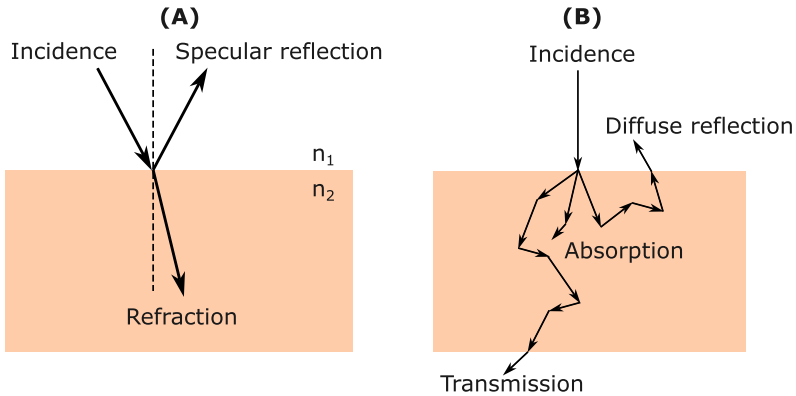
Figure 1.1 Basic effects of light-tissue interactions: (A) At the air-tissue interface: specular reflection and refraction (where $n_2 > n_1$). (B) propagation of light through tissue: absorption, transmission, and diffuse reflectance.
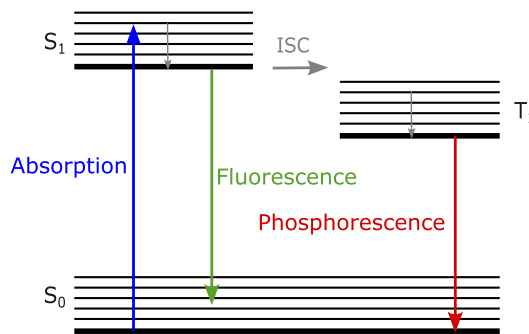
Figure 1.2 Example Jablonski diagram illustrating the fundamental processes of fluorescence and phosphorescence. ISC: intersystem crossing; S_0: ground state; S_1: excited singlet state; T_1: metastable state.

and normal tissue, classification of different types of tissues in the body, to determine physiological conditions, such as hydration level of tissue. RI values help us understand tissue pathology which is critical to the computation of power and intensity (and often wavelength) of light required for a certain application. Refraction and reflection occur due to variations in refractive indices as light travels through different media. Refraction is governed by Snell's law:

$$v_1 sin(\theta_1) = v_2 sin(\theta_2).$$

In this equation, v_1 and v_2 are speeds of light in medium 1 and medium 2, respectively; θ_1 is the angle of incidence of light on medium 2 when entering from medium 1, and θ_2 is the angle of refraction (how much the light bends after entering medium 2). The refractive index n of a medium is related to speed of light in that medium by the equation:

Optical biosensors: from working principles to detection methods of label-free devices

2

Tatevik Chalyan[a], Heidi Ottevaere[a], and Laura Pasquardini[b]
[a]Brussels Photonics (B-PHOT), Department of Applied Physics and Photonics, Vrije Universiteit Brussel, Brussels, Belgium, [b]Indivenire srl, Trento, Italy

2.1 Biosensors

A biosensor is a complex mingled device providing specific quantitative or qualitative analytical information on a sample through a biological recognition element that is in direct contact with a transduction element [1]. It is a manifold system connecting different fields, such as biology, chemistry, optics, electronics, and informatics in a single device. In 1975 the first commercial biosensor to analyse whole blood glucose content was reported [2]. Since then, biosensors technology started, with the development of different components of the whole system, improving the performance and specificity of biosensors, as well as including new targets for detection. Fig. 2.1 shows the key components of any biosensing device.

In most of the case to detect the target molecules, i.e., the analyte, the transducer element is derivatized (activated) with specific molecules, so called ligands or receptors,
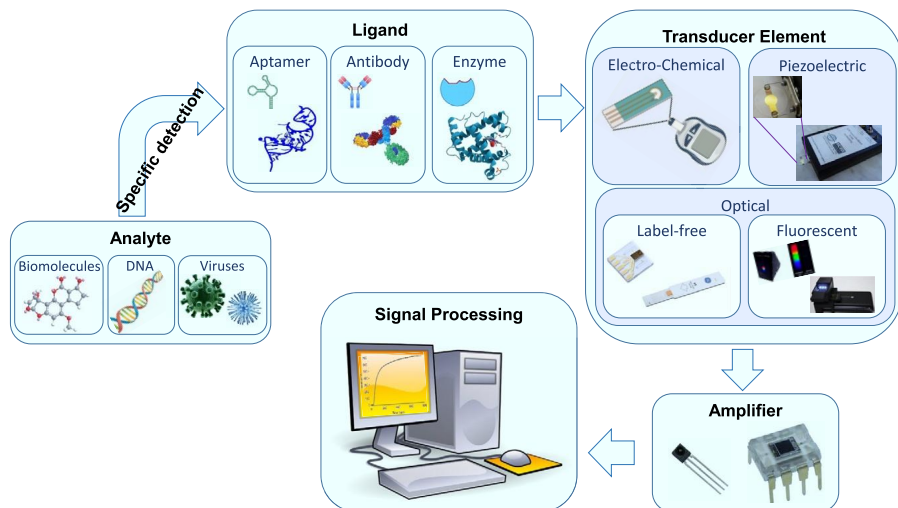

Figure 2.1 Key components of a biosensor: The transducer receives a signal from a ligand-analyte reaction, which is read as an electrical/optical signal in real time.

Figure 2.6 Representation of the SPP modes. (a) The nature of the modes arising from metal-dielectric interference. (b) The evanescent fields in the two media.

Now, let us recall the sensing techniques based on plasmonic effects. In any SPR configuration, the incident light totally reflects from the dielectric-metal surface and generates an evanescent field penetrating into the metal layer. Under certain angles or wavelengths, the propagation constant of the evanescent field matches with SPP, resulting in a resonance coupling of the incident light with SPP. This yields an intensity loss in the output reflected light and the appearance of a characteristic negative peak (dip) in the intensity profile of the reflected light as a function of the incident angle. The position of the dip, and consequently of the resonance angle, is correlated with the refractive index near to the metal surface. Thus a change in the surrounding environment yielding a change in the refractive index causes the displacement of the resonance angle, which is measured by the shift of the intensity dip. In particular, using a metal surface as a layer for ligand molecule immobilization, and flowing a target solution over that layer, the molecular binding event can be monitored by recording the angular position of the intensity dip [36]. Numerous commercial products exist based on the SPR method. The most known and commonly used are the *Biacore*[3] instruments, which are totally automated, so that the analysis and the sensor regeneration is computer controlled. The sensor chip in Biacore systems, consists of a glass slide coated with gold permitting to monitor binding events between molecules, ranging from ions to viruses.

2.2.3 Waveguide based biosensors

Waveguide-based optical biosensors represent a large class of detection mechanisms, which include a variety of optical structures, such as interferometers, resonators, etc. The introduction of waveguides by Colladon dates back to 1842, who experimentally showed that due to total internal reflection (TIR), the light can be guided in a transparent material with a refractive index higher than its surrounding environment ($n_{substrate} < n_{core} > n_{clad}$) [37]. By using waveguides, the light path can be simply controlled without the necessity of using bulky components, such as mirrors or beam

---

[3] https://www.gelifesciences.com/en/ae/solutions/protein-research/products-and-technologies/spr-systems.
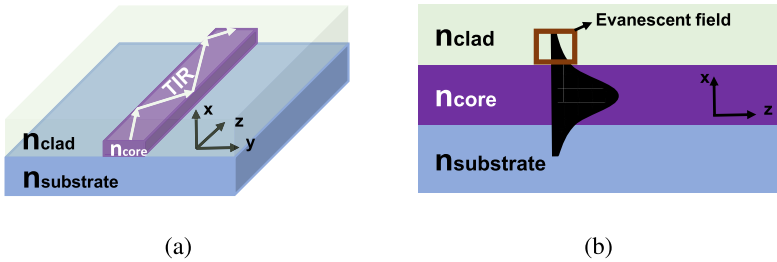
Figure 2.7 Schematic of a slab waveguide. (a) The total internal reflection takes place in a wave-guide when the $n_{substrate} < n_{core} > n_{clad}$ condition is satisfied. The propagation direction is z. (b) The evanescent field penetrates into the cladding layer, thus becoming sensitive to environmental changes.

splitters (see Fig. 2.7a). Light propagation through waveguides offers excellent possibilities for sensing. Light propagates through the waveguide according to particular patterns of the electromagnetic field, called guided modes [38]. In a slab waveguide the electric component of the guided mode is given by

$$\bar{E}_i(x, z, \omega, t) = \bar{E}_i^0(x, \omega) \exp[j(\omega t - \widetilde{\beta}_i z)], \tag{2.13}$$

where z is the propagation direction, and x is the direction in which the refractive index step profile occurs. The field profile $\bar{E}_i^0$ and the propagation constant $\widetilde{\beta}_i$ of mode i are dependent on the light angular frequency ω, the geometry and the refractive index n of all the materials (see Fig. 2.7b).

Let us define the effective refractive index $\widetilde{n}_{eff_i}$ of the mode as

$$\widetilde{\beta}_i = \frac{2\pi}{\lambda} \widetilde{n}_{eff}, \tag{2.14}$$

where λ is the wavelength of the propagating light.

In addition, for a certain combination of these parameters, one can achieve monomode waveguiding systems that have only one transverse electric (TE) or transverse magnetic (TM) guided-wave.

What is important for sensing is the fact that $\bar{E}_i^0(x, \omega)$ is not to be strictly confined to the core layer, but has exponentially decaying tails in the surrounding materials as well; these are named the evanescent fields. The decay length of the evanescent field ranges from one tenth of the wavelength to infinity, depending on the geometry and materials. Nevertheless, there is a large interaction volume of the evanescent field with the surrounding materials. This is used in sensing, since each change in these materials is sensed by the propagating optical modes and can be measured as a change in their characteristics. In most chemo-optical sensors, the sensing action is localized in the cladding region. As the evanescent field of the guided mode penetrates into the cladding, any refractive index change near to the waveguide surface yields a

Fluorescence microscopy: backbone of modern biomedical research 3

Andrey Andreev[a], Evgenia V. Azarova[b], and Jeremy Delahanty[c]
[a]Division of Biology and Biological Engineering, California Institute of Technology, Pasadena, CA, United States, [b]Department of Materials Science and Engineering, Johns Hopkins University, Baltimore, MD, United States, [c]Department of Neuroscience, Johns Hopkins University School of Medicine, Baltimore, MD, United States

3.1 Fluorescence phenomena: photons in, photons out

Fluorescence microscopy helps us study organic and inorganic substances and biological processes. It is essential to understand the phenomena behind the term "fluorescence," the physical process in which photons (also often referred to as light particles or light waves) are first absorbed and then emitted. Each photon represents the quantum form of electromagnetic radiation. The most common form is known as visible light, a small portion of the electromagnetic radiation spectrum that the human eye can detect.

The term itself was first introduced in 1852 by English mathematician Sir George G. Stokes, even though the phenomenon was first observed in 1845. The compound used to make the discovery was plant-derived antimalaria chemical quinine (also used as flavoring in tonic water), an aromatic molecule that could absorb and emit light. Since this observation, scientists have learned how to synthetically create fluorophores for various purposes, including biomolecular visualization. The absorption and emission of light are commonly illustrated by the Jablonski diagram (Fig. 3.1). The diagram has a set of horizontal lines representing various permitted energy levels of the molecule and a set of arrows that represent the transitions between different electronic states that occur when a molecule is photochemically activated.

To better understand the physics of fluorescence, consider a fluorescent compound that has been in its resting ground state (S_0). After interaction with the light particles, our fluorescent compound can absorb the energy from these photons, causing a valence electron to migrate from its resting state to one of the higher energy states (e.g., S_1, S_2). This transition is called "excitation"; as shown on the Jablonski diagram, it is often represented by the arrow pointing up. When an electron jumps to its higher energy state, it starts rapidly losing some of the absorbed energy by moving from a higher to a lower energy state. This process is represented by curved arrows and is referred to as vibrational relaxation, followed by light emission. The entire process usually takes on the order of nanoseconds.
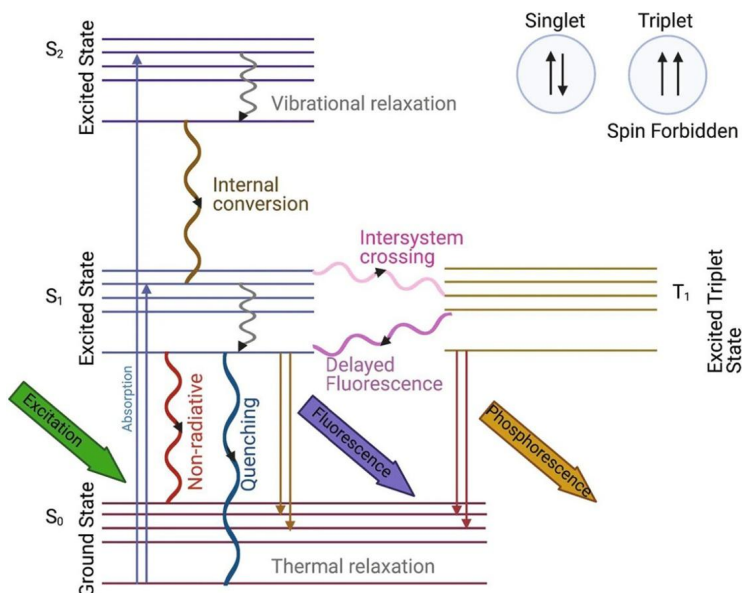
Figure 3.1 Diagram depicting energy levels in a molecule and potential transitions is a useful tool to conceptualize fluorescence and associated physical phenomena. Molecules have wide absorption spectra reflected in several excited states. Similarly, the system can relax to ground state by emission from several different states. Vibrational relaxation is one of the types of energy losses that lead to the emission spectrum being more "red-shifted" (photons with less energy) than absorption spectrum. Adapted from [1].

3.1.1   Multiplexity through fluorescence

Various fluorophores absorb and emit light at different wavelengths, allowing us to differentiate multiple objects of study. For example, we can use fluorescence to investigate protein complexes by labeling subunits within the complex with nonidentical fluorescent molecules [2]. Specificity of fluorescence allows us to visualize and analyze several targets in the same experiments. However, to achieve that easily, the fluorophores have to be "spectrally separated," that is, their excitation and/or emission spectra has to be sufficiently different. Due to spectral overlap between fluorophores, we can usually separate up to 3 fluorophores using conventional optics and without computational processing. Algorithms of spectral unmixing [3] [4] allow separation of up to seven fluorophores, some of which might have significant overlap in spectra.

Unmixing several fluorophores is limited by the ability to resolve different spectral "bins," for example, through resolution of spectral linear detectors. The amount of signal in each "bin," more specifically, signal-to-noise ratio, defines bleed-through between channels after unmixing. Thus hyperspectral imaging, especially when unmixing more than 3 (usually) channels, might require a high amount of signal to be collected, and concomitantly, longer exposure time, slower imaging, or higher laser power. Hyperspectral imaging might be more useful not for live imaging, but for multitarget quantification for diagnostics; this will be discussed in a later section.

1. Chemical covalent bonds between molecule and fluorophore
2. "Click" chemistry between fluorescent molecule and target molecule
3. Intermediate genetically-encoded tags, such as biotin-avidin system
4. Direct fusion of genetically-encoded fluorescent protein with protein of interest
5. Tagging specific toxins, such as phalloidin for labeling actin

Using fluorophores of different spectral properties ("colors"), one can tag several molecules in the same context and measure their relative characteristics. Ideally, we want to only use orthogonal labels, that is, fluorophores with significant spectral separation. Hyperspectral unmixing (discussed earlier) allows an increase in the number of targets that can be recorded simultaneously. Here we review several examples of using specificity of fluorescence for biomedical applications.
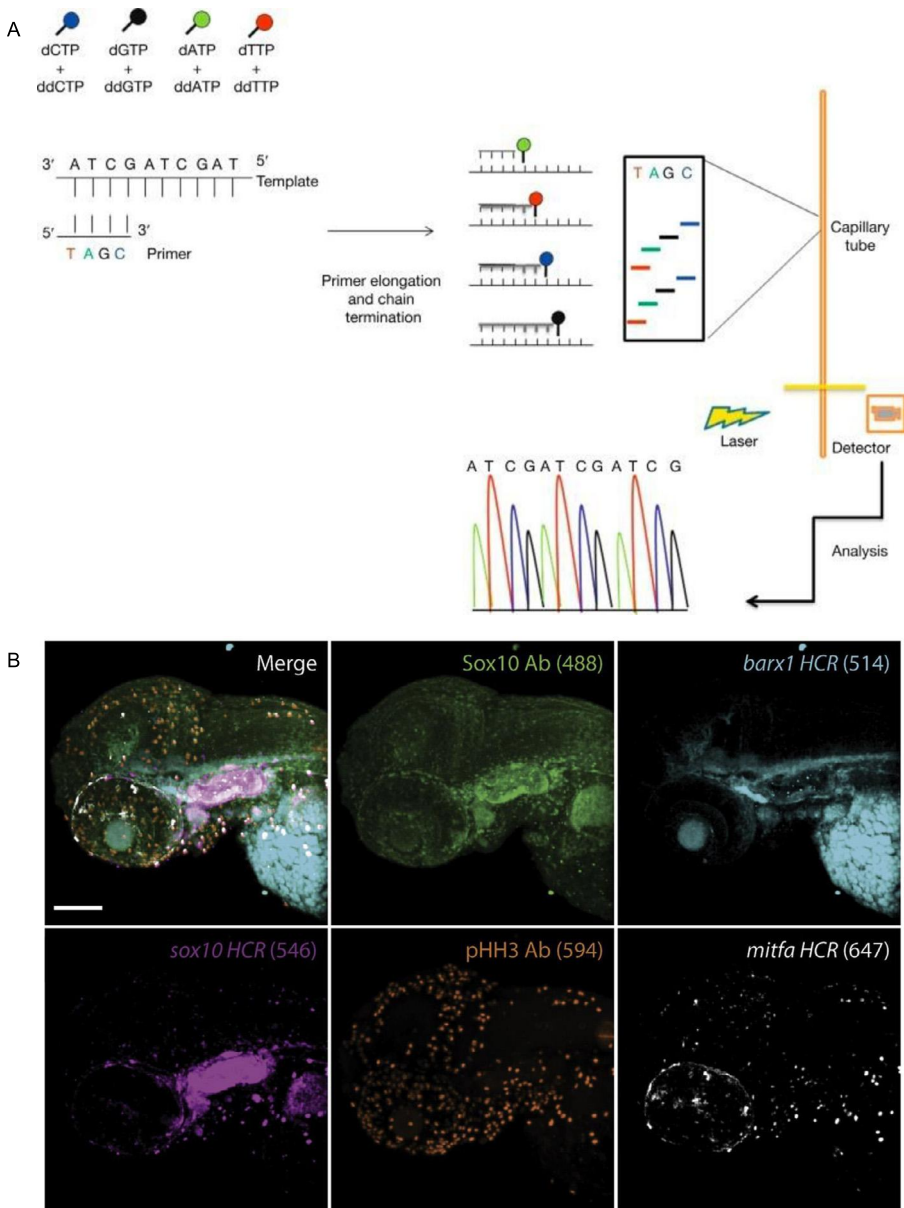
3.3.1   Genomic analysis

Monumental effort has been made to finish sequencing of the human genome. Fluorescence played an important role in completing this task. Following the Sanger sequencing approach [40,41], which requires radio isotopes, a similar method based on automatic detection of nucleotide bases using fluorescence was developed in 1984 [42]. In this approach, DNA is synthesized using a mixture of normal bases and synthesis-terminating nucleotides labeled with fluorophores. Each such terminating nucleotide (dideoxynucleotides or ddNTPs) carries different fluorophores, for example, adenine (A) is labeled with fluorescein, thymidine (T) is labeled with Texas-Red, and so on. DNA molecules are synthesized using polymerase, and whenever a synthesis-terminating base is incorporated, it truncates a given copy of DNA. Thus, the reaction solution ends with an assortment of truncated DNA molecules terminated with a specific fluorophore (Fig. 3.5). That fluorophore "color" allows detection of the terminated base, and separation of DNA molecules on gel electrophoresis allows reconstruction of the sequence.

Application of fluorescence for DNA sequencing improved specificity and efficiency, it also removed requirements for radioactive compounds, and allowed automation of sequencing. A variation of Sanger sequencing is still used in practice, for example, to verify sequences of short DNA fragments; however, whole-genome sequencing progressed to next-generation sequencing (NGS), which also relies on fluorescence detection [45].

3.3.2   Spatial-omics: imaging meets diagnostics

Though genome sequencing and genetic testing are crucial tools for clinical work, we also need to be able to quantify expression of the genes of interest. After effectively solving the technical problem of "genome" sequencing, modern diagnostics are now focusing on problems of "exome" characterization, or distribution of RNA molecules within tissues (transcriptome). Out of several approaches, two tools for spatially-resolved transcriptomics are leading [46]. First, is a fluorescent *in situ* hybridization [47,48], which labels RNA molecules of interest with a fluorophore-labeled probe

Figure 3.5 Applications of fluorescence for clinical diagnostics. (A) Specificity of fluorescence allows labeling of individual DNA bases for precise sequencing [43]; (B) Microscopic imaging of tissues labeled with set of probes targeting expression of specific transcripts (mRNA) allows characterization of tissue state with sub-cellular resolution in zebrafish embryo [44].

Raman spectroscopy—research lab analytics

4

Oleksii Ilchenko[a,b], Andrii Kutsyk[b,c,d], Zhongyang Zhang[a], and Anja Boisen[a]
[a]Technical University of Denmark, Department of Health Technology, Center for Intelligent Drug Delivery and Sensing Using Microcontainers and Nanomechanics, Kgs. Lyngby, Denmark, [b]Lightnovo ApS, Birkerød, Denmark, [c]Department of Energy Conversion and Storage, Technical University of Denmark, Kgs. Lyngby, Denmark, [d]Faculty of Radiophysics, Electronics and Computer Systems, Taras Shevchenko National University of Kyiv, Kyiv, Ukraine

4.1 Introduction

Since the discovery of the Raman effect in 1928 Raman spectroscopy has become a powerful tool that provides information about the molecular structure and composition of materials with numerous fields of application. The Raman effect is a type of inelastic light scattering by molecules. It was predicted by A. Smekal in 1923 [1] and was observed experimentally in liquids by C.V. Raman and K.S. Krishnan [2]. G.S. Landsberg and L.I. Mandelstam observed it in quartz crystal [3].

The Raman spectrum contains unique fingerprint-like features that allow the identification and characterization of different molecular species. One of the key advantages of Raman spectroscopy is its nondestructive nature, which makes it suitable for the analysis of delicate or sensitive samples. Unlike other techniques, such as infrared spectroscopy, Raman spectroscopy does not require sample preparation that could alter the sample's properties. Additionally, Raman spectroscopy can be performed in a variety of sample environments, including gases, liquids, and solids, making it a versatile technique for studying a wide range of materials.

Advances in instrumentation have expanded the capabilities of Raman spectroscopy. The invention of laser, the introduction of sensitive charge-coupled devices for the detection of scattered light and filters for the rejection of elastically scattered light have made Raman spectroscopy a widespread laboratory technique. The development of confocal Raman spectroscopy has enabled high-resolution imaging of samples and has allowed obtaining spatially resolved chemical information. This has found applications in material science [4,5], pharmaceutics [6–9] as well as in biological sciences, where Raman imaging can be used for cellular imaging [10,11] and studying tissue composition [12,13].

Another important development in Raman spectroscopy are the techniques known as surface-enhanced Raman spectroscopy (SERS) [14] and tip-enhanced Raman spectroscopy (TERS) [15]. SERS relies on the interaction between molecules and metallic nanostructures, which leads to a significant enhancement of the Raman signal. This technique has revolutionized the field of Raman spectroscopy by enabling high sen-

Subwavelength periodic dielectric nanostructures for biochemical sensing

5

Leonid Beliaev, Osamu Takayama, and Andrei Laurynenka
DTU Electro – Department of Electrical and Photonics Engineering, Technical University of Denmark, Kongens Lyngby, Denmark

5.1 Introduction

A sensor is an analytical tool that can detect and respond to physical input from its environment and convert it into a measurable optical or electrical signal. A typical sensor has three parts: a recognition element, a transducer, and a signal processing part. Sensors can be used in various fields, such as medicine, environmental monitoring, and biotechnology. Each application has specific requirements for measuring the analyte, including concentration, precision, sample volume, and time required to complete the probing. Sensor devices can be classified into different groups, depending on the signal transduction method: electrochemical, acoustic, optical biosensors, etc. In this chapter, we focus on the latter read-out scheme. Optical sensors measure variations in light properties, such as polarization, intensity, and wavelength, as the reaction on biological or chemical interactions [1]. They can be divided into two categories: label-based and label-free. Label-based optical sensing uses special "labels" to generate an optical signal, whereas label-free sensing generates the signal directly through interactions between the analyzed material and the transducer. Optical sensors offer advantages over other conventional analytical techniques, such as direct detection of substances in real-time, high specificity, sensitivity, small size, and cost-effectiveness. Optical sensor miniaturization allows chip-level integration, and lab-on-a-chip devices can also incorporate other functionalities, such as microfluidics [1].

Nowadays, one of the most widely used and commercialized optical sensors is a plasmonic device [2], where noble metals, such as gold (Au), silver (Ag), and copper (Cu), are usually used as plasmonic materials with negative permittivity [2–4]. Gold is most popular due to its optical properties in the visible to infrared (IR) wavelength ranges, chemical resistance, and well-developed biofunctionalization procedures [3]. Metals, however, have several disadvantages as sensing materials. Though gold is stable in the air, other metals, such as silver and copper, can degrade due to oxidation and moisture [5]. Plasmonic sensors based on metals also have a limited spectral operation range and suffer from losses at optical frequencies, which can cause heating and affect the refractive index of the medium under study [6]. In addition, the plasmonic properties of metals are difficult to tune or adjust [5], and metals, as a rule, are not cleanroom compatible.
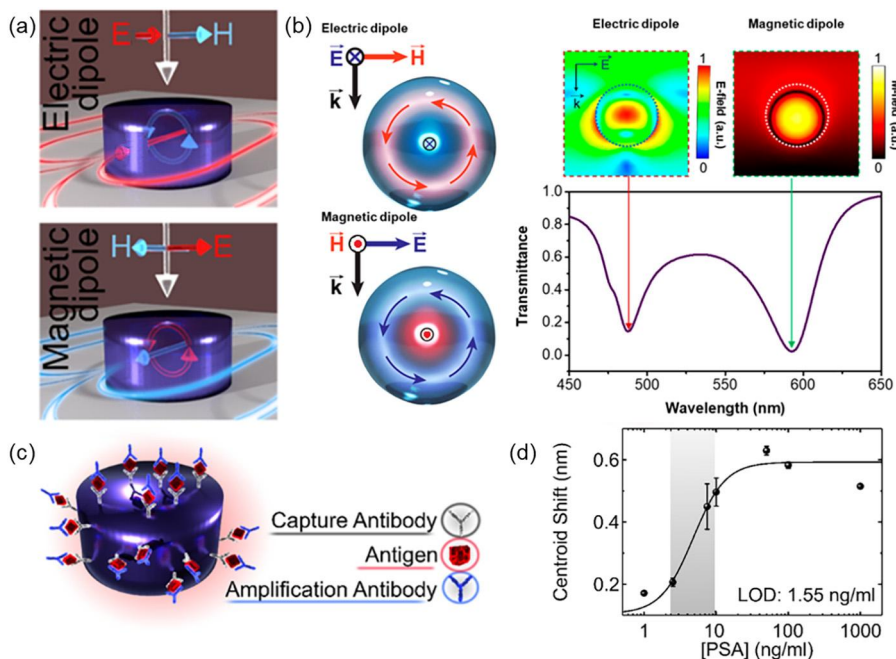
Figure 5.6 Mie resonance for refractometric sensing. (a) Schematic illustration of electric and magnetic dipoles in dielectric discs. Adapted with permission from ref. [110]. Copyright 2019, American Chemical Society. (b) dielectric spheres, field profiles, and transmission spectrum of a 150 nm Si spherical nanoparticle. Adapted with permission from ref. [8]. Copyright 2021, American Chemical Society. (c) Illustration of Si disc for biosensing and (d) sensitivity curve. Adapted with permission from ref. [110]. Copyright 2019, American Chemical Society.

tive index. Bulk refractive index sensitivity mostly ranges from ten to several hundred nm/RIU for these dielectric-based metasurfaces. At the same time, plasmonic sensors typically exhibit one order of magnitude larger bulk sensitivity [3]. We can also conclude that apart from Si, there are two mainstream materials used for visible and near-IR wavelengths, namely, titanium oxide and silicon nitride, for their transparency and relatively high refractive indices.

In this section, we discuss one example of dielectric metasurfaces used for gas detection by the refractometric sensing scheme. Hydrogen gas sensing can be realized by aluminum-doped zinc oxide (Al:ZnO, AZO) nanotube metasurfaces, as shown in Fig. 5.7(a) [114]. Hydrogen (H_2) is a highly combustible gas with low ignition energy. A concentration exceeding 4% is hazardous, as hydrogen can easily explode. Since H_2 is a tasteless nontoxic gas, it is hard to detect by human senses and requires hydrogen sensors for safety. Hydrogen gas can be detected by the electrical readout. However, as higher than 4% concentrations of hydrogen can ignite with a small spark, electrical detection is used below the 4% concentration. Therefore a low-power optical detection is desired. The dimensions of each AZO tube are the following: 2000 nm in height and 300 nm in diameter with a wall thickness of 20 nm. The nanotubes are arranged in a
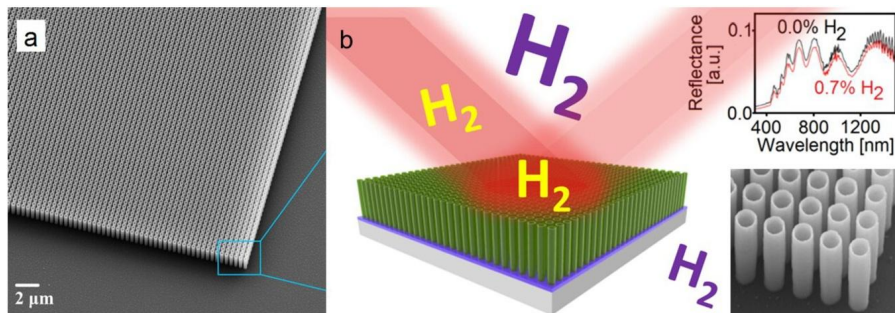
Figure 5.7 Dielectric metasurfaces for hydrogen gas detection by refractometric sensing. (a) Scanning electron microscope (SEM) images of the fabricated aluminum doped zinc oxide (AZO) nanotubes with a pitch of 400 nm, diameter of 300 nm, and height of 2 μm. The wall thickness of nanotubes is approximately 20 nm. (b) Illustration of hydrogen sensing by reflection spectrum. Adapted with permission from ref. [114]. Copyright 2020, Royal Society of Chemistry.

square lattice with 400 nm period. Such high aspect ratio nanostructures can be fabricated by the combination of deep ultraviolet (DUV) lithography, dry etch, and atomic layer deposition (ALD) techniques [115–120].

The underlying principle for hydrogen detection in this metasurface system is a Fabry-Pérot resonance in tubes when light reflected from the top of the tubes (air-tube interface), and from the bottom (tube-substrate interface) interact constructively and destructively, resulting in sinusoidal reflection spectra. The spectral positions of reflection dips and peaks depend on the height of the layer (tubes) and its effective refractive index. Being exposed to hydrogen absorbed at the surface of the tubes AZO slightly changes its refractive indices, depending on the concentration of hydrogen, which leads to the red-shift of the spectrum as shown in Fig. 5.7(b). The spectral shift was observed for the thin wall tube structures due to a large surface-to-volume ratio. It is absent for AZO solid pillars. The AZO nanotubes show a spectral shift of 13 nm upon exposure to H_2 gas with 4% concentration at room temperature within 10 minutes.

5.3 Fluorescence sensing

Photoluminescence (PL)-based detection techniques have been widely used in chemistry, biology, materials science, and medicine to label biomarkers for sensing or a certain part of biological objects for imaging. However, a weak optical signal from a single luminophore limits sensitivity, making it a critical problem in the detection of biomarkers in low concentrations in applications such as DNA sequencing, drug screening, and early diagnosis [121,122]. To address this challenge, technologies that amplify fluorescence signals are being pursued to improve sensitivity for such label-based sensing schemes [123]. One extensively studied approach is the manipulation of photoluminescence, which has been shown to significantly enhance the PL intensity when photon emitters are coupled to an optical cavity or when located near the intense

Integrated photonic and plasmonic biosensors

6

M. Imran Cheema[a] and Faiza Iftikhar[b]
[a]Electrical Engineering Department, Syed Babar Ali School of Science and Engineering, Lahore University of Management Sciences (LUMS), Lahore, Pakistan, [b]Electrical Engineering Department, Lahore College for Women University, Lahore, Pakistan

6.1 Introduction

Can we have devices similar to commercial glucometers and pregnancy testers for diagnosing any disease rapidly, accurately, and in point-of-care settings? Yes, we will have such devices for many diseases in the future, and one of the promising directions to realize such diagnostic tools is integrated photonics and plasmonic biosensors. Integrated photonics and plasmonic sensors offer various advantages, such as small footprints, low detection limits, analyte detection multiplexing, and compatibility with the CMOS technology. That is why these platforms have gained much attention in recent years for realizing various biophotonics and biosensing applications, including point-of-care diagnostics.
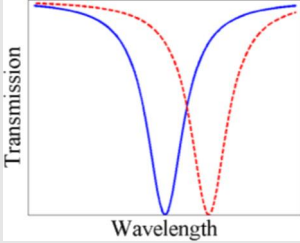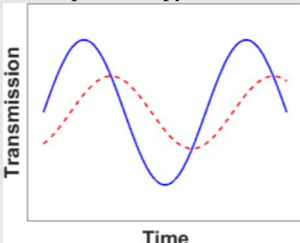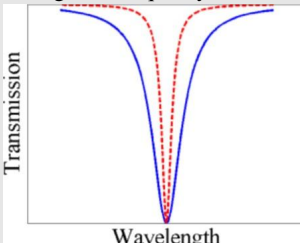
Currently, health diagnostics require expensive infrastructures, specialized personnel, time-consuming procedures, and in many cases, long result times. In low and middle-income countries, the diagnostics landscape is even more challenging due to a lack of resources, support personnel, and finances. Therefore there is a critical need for rapid, cost-effective, easy-to-use, and accurate biosensors globally. A recent worldwide market insights research report indicates that the global biosensors market is expected to reach USD 49.6 billion by 2030 [1]. We anticipate that integrated photonics and plasmonic biosensors will be a significant part of the healthcare ecosystem in the next few years.

This chapter presents an overview of the evanescent field detection-based photonic and plasmonic biosensors, emphasizing their fundamental principles, architectures, and applications. We also briefly discuss the crucial components of biosensors, namely surface functionalization, and microfluidics.

6.2 Biosensor surface functionalization
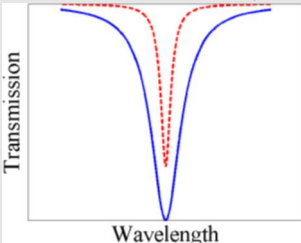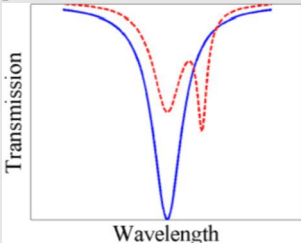
In an integrated photonic and plasmonic biosensor, analytes attach to the sensing surface through surface functionalization [2]. This process involves preparing or modifying the sensor's surface to allow the analyte to bind in the correct orientation for improving sensitivity. Additionally, surface functionalization helps to prevent the sensor's fouling and enables its reusage through regeneration. The process of increasing selectivity by allowing the sensor to bind the desired analyte while blocking unwanted substances in the sample is known as antifouling [3]. The surface functionalization

Table 6.1 Comparison of major techniques used to track changes in properties of a microcavity as a function of sensing events.

Technique	Implementation	Pros	Cons
Change in the resonant wavelength Red dip due to the sensing event	(i) Track the minimum of the resonant peak directly [35]	Simplest implementation and real-time.	Ignores absorption of a sensing event; signal depends upon a sensing event's location along the mode profile; noise sources, such as laser intensity fluctuation and wavelength instability
Change in the quality factor using phase shift cavity ring down spectroscopy 	Send a sinusoidally modulated laser light into the cavity and monitor the phase shift of the output light as a function of the sensing event [18]	No noise sources, such as laser intensity fluctuation and wavelength instability; sense both mode effective index change and absorption due to a sensing event [20,36]	The signal depends upon a sensing event's location along the mode profile; implementation is relatively more involved compared to the resonant wavelength tracking
Change in the quality factor 	Fit the resonant peak to a Lorentzian function, and then extract the quality factor [37]	Sense both mode effective index change and absorption due to a sensing event	Nonlinear curve fitting; fit error due to the assumed Lorentzian function; signal depends upon a sensing event's location along the mode profile; noise sources, such as laser intensity fluctuation and wavelength instability

Table 6.1 (*continued*)

Technique	Implementation	Pros	Cons
Change in transfer characteristics of the cavity	Monitor the resonant peak strength [38]	Simpler implementation and real-time	Primarily for absorption measurements; signal depends upon a sensing event's location along the mode profile; noise sources, such as laser intensity fluctuation and wavelength instability
Splitting of the single resonant peak into a doublet	Fit the doublet to a two-peak Lorentzian function and extract the two resonant wavelengths and their separation [39]	Signal independent of a sensing event's location along the mode profile	Nonlinear curve fitting, primarily demonstrated for sizing of solid particles; fit error due to the assumed Lorentzian function; noise sources, such as laser intensity fluctuation and wavelength instability

trinsic to the cavity material. Active WGM biosensors can probe analytes with their ultranarrow resonant linewidths and consequently offer highly sensitive and lower detection limit biosensing mechanisms. Their interrogation systems can be realized without tunable lasers and, as a result, can be relatively low-cost compared to passive WGM biosensors [48].

A range of biosensors have been demonstrated using integrated and active WGM cavities. For example, active microdisk resonators have successfully detected protein rhS100A4 [48] and Human IgG [49], illustrating their proficiency in protein sensing. Microtoroid resonators with gain media have demonstrated their potential by detecting influenza virus in the air [50], offering a promising avenue for airborne virus detection.

6.5.2.3 Fabry-Pérot (FP) cavity biosensors

Integrated FP cavities consist of two mirrors that are generally in the form of polished surfaces or Bragg reflectors. In contrast to WGM cavities, FP cavities are usually linear geometry. In FP cavities, integration of fluidics, i.e., sample delivery, is relatively

Optical fiber-based biosensing: applications in biology and medicine

7

Linhui Yu[a,b,d], Radhika K. Poduval[a,b,d], and Kartikeya Murari[c]
[a]Massachusetts General Hospital, Boston, MA, United States, [b]Harvard Medical School, Boston, MA, United States, [c]University of Calgary, Calgary, AB, Canada

7.1   Introduction

Optical biosensing is a powerful technique that uses the modulation of properties of light (intensity, wavelength, phase, polarization, etc.) to measure biomarkers. Endogenous properties of biological tissue, e.g., scattering, absorption, birefringence, etc., are rich in valuable structural and functional information, which can be measured by optical sensing. Moreover, researchers can engineer optical solutions with highly specific contrast enhancements to target a wider range of biomarkers, making optical sensing an even more versatile tool for biomedical research.

Optical biosensing has been demonstrated and explored as a potential tool in various clinical settings, including intraoperative guidance, vital sign monitoring, disease diagnosis, and treatment monitoring. Additionally, it is a valuable technique in basic research, enabling the investigation of biological processes and disease mechanisms across biological models, such as animal models, cell and tissue cultures, organoids, and various body fluid samples, e.g., blood, saliva, and urine.

When using light for biomedical sensing, particularly in *in-vivo* applications, there are two major challenges: i) to overcome tissue scattering, which restricts the depth of penetration, and, ii) the difficulty of accessing body parts that are anatomically out of reach for bulk optics.

Optical fiber sensors provide a robust approach to overcoming challenges in biomedical optics due to their small footprint and flexibility. Fiber optics-based probes and endoscopes can access hard-to-reach body parts and cavities, such as the gastrointestinal tract, coronary artery, and respiratory system. Small-diameter fiber probes can be passed through needles and catheters, providing optical access to deep tissue structures that are otherwise unreachable with minimal invasiveness. Moreover, the optical fiber sensors can be made biocompatible to interact safely with living tissue without causing harm or rejection.

This chapter offers an overview of the current state of fiber-based biosensing. Section 7.2 reviews the fundamental principles of fiber optics, including single-mode and multimode fibers, as well as some examples of specialty fibers. Additionally, we dis-
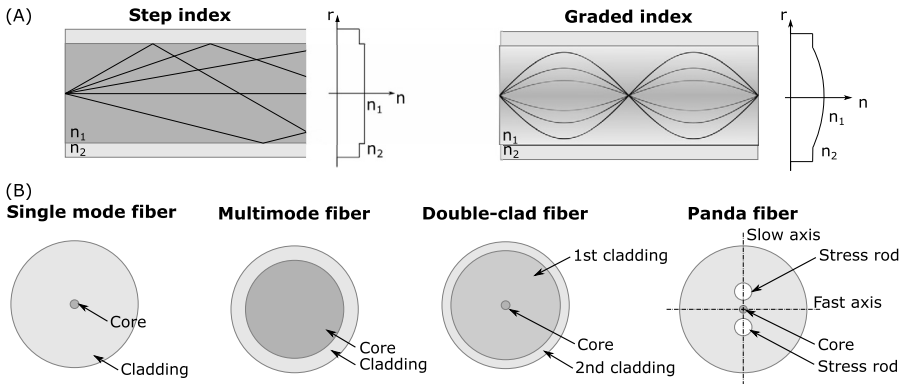
---

[d] Equal contribution.

Figure 7.1 (A) Fiber core composition of step index and graded index fibers and their refractive index profile. (B) Cross-sectional view of some different optical fiber types. Darker shaded color indicates higher refractive index.

cuss fiber modifications that can enhance illumination and collection in fiber-based sensing. In Section 7.3, we present an overview of major fiber-optics-based biosensing technologies, such as diffuse reflectance spectroscopy for measuring intrinsic properties of biological tissue, fiber photometry and fluorescence fiber probes for measuring fluorescence markers, and interferometric sensing for sensing pressure and temperature. For each technique, we overview the principles, hardware considerations, and biosensing parameters that can be measured by optical fiber-based systems. Lastly, Section 7.4 outlines the future prospects for fiber-based sensors and systems.

7.2   Principles of fiber optic sensors
7.2.1   Optical fibers

Optical fibers transmit light from one end to the other, with light traveling in the core via total internal reflection. An optical fiber consists of a central core surrounded by cladding, in which the refractive index of the cladding material is lower than that of the core.

Optical fibers can be classified into two types based on their core composition: step-index and graded-index fibers, as shown in Fig. 7.1 (A). Step-index fibers have a core with a constant refractive index higher than the cladding. Light travels through the core in a straight path, with reflections occurring at the core-cladding interface. Graded-index fibers, on the other hand, have a core with a varying refractive index, which gradually decreases from the center of the core to the cladding. As a result, light bends smoothly through the fiber instead of being reflected at the core-cladding boundary. The index profile of graded-index fibers is designed to minimize the difference in the axial propagation speed of rays in the fiber.
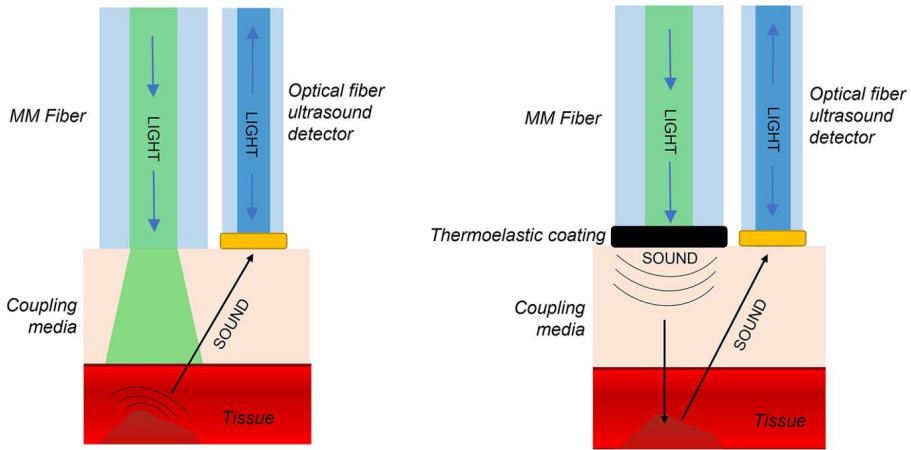
(A) Photoacoustic Imaging   **(B) Optical Ultrasound Imaging**

Figure 7.9 Schematic illustration of two prominent fiber-optic all-ultrasound imaging schemes. (A) **Photoacoustic Imaging**, where tissue is illuminated by light from an optical fiber, which photoacousticaly generates ultrasound energy which is detected by a fiber-optic ultrasound detector. (B) **Optical Ultrasound Imaging**, where laser-generated ultrasound produced at the endface of an optical fiber with a thermoelastic coating is directed at the tissue of interest, and the ultrasound echoes are detected by a fiber-optic ultrasound detector. MM: Multimode.

sound waves that can propagate to the tissue of interest, and the ultrasound echoes can be detected through a second colocated fiber-optic pressure sensor.

Both these fiber-optic imaging schemes use distinct "transmission fibers," but the pressure sensors for ultrasound reception have largely similar properties and are often used in both modalities PAT and optical ultrasound. Both PAT and optical ultrasound transmitters use laser beams guided through MM fibers with wavelengths ranging from visible ~532 nm to NIR ~1064 nm [56,79]. The associated ultrasound detectors however tend to be constructed as fiber-optic Fabry-Perot interferometers interrogated by NIR light in the 1500 nm to 1600 nm range [56,93].

Several groups have managed to fabricate fiber-optic ultrasound generators. Tian et al. reported an ultrasound transmitter fabricated by a focused ion beam technique, wherein highly absorptive Au nanopores were patterned on the end face of an optical fiber [94]. The miniature optical ultrasound transmitter produced ultrasound with an amplitude of 2.7 kPa and a -3 dB bandwidth of 7 MHz. Another fiber-optic transmitter using Au was fabricated by Zou et al. using a composite synthesized by mixing the AuNPs into PDMS following single-step synthesis protocol, and dip coated on a multimode fiber with a core diameter of 400 μm to realize a broadband miniature fiber-optic optical ultrasound transmitter [95]. The generated ultrasound had an amplitude of 0.64 MPa and a bandwidth of more than 20 MHz, which were

Photonic biosensing at the point-of-care

8

Daniel J. Steiner, Michael R. Bryan, and Benjamin L. Miller
Department of Dermatology, University of Rochester, Rochester, NY, United States

8.1 Introduction: the need for PoC biosensing

Diagnostic technology is becoming as familiar to consumers as the cell phone, and in some cases actually *is* the cell phone. Whether it's the watch-integrated heart rate and step count monitors many of us wear 24 hours a day, to the COVID-19 lateral flow assays (LFAs), which became ubiquitous over the course of the SARS-CoV-2 pandemic, people have access to dramatically more information about their health than previously thought possible. However, despite this avalanche of new consumer-grade technology, there is still a tremendous amount of diagnostic information not available at the consumer level, or even in a doctor's office. To bridge that gap and bring us ever closer to the "tricorder" idea popularized in *Star Trek*, researchers in academia and industry around the globe are developing new technologies suitable for use at the point-of-care (PoC).

The need (and consumer desire) for at-home and PoC diagnostics has grown as populations age, infectious diseases emerge, and technology expands. Individuals today are increasingly aware of their personal health status and understand the role that information has in healthcare. To meet this global need for health monitoring, there emerged an increased pressure for innovation and technological advancement. Many large biomedical companies saw this need and began to expand their operations to include dedicated PoC programs, especially since the 2019 SARS-CoV-2 pandemic. While established entities were refocusing their efforts to bring PoC capability to product menu, diagnostics became a central focus for a variety of academic research laboratories that realized their unique approaches and technology (culminating in intellectual property) could be repurposed (or created *de novo*) to further our understanding and the development of technologies that would be deployable at the PoC.

Beyond the need for PoC systems in the doctor's office and at home, there are many other environments where easy-to-use, rapid diagnostic technology has the capacity to impact lives. For example, the exhaustion of emergency department (ED) personnel, resources, and time is recognized as a significant healthcare problem. This results in a situation where the "identified need for emergency services exceeds the available resources for patient care in the ED, hospital or both," which is the definition of overcrowding as provided by the American College of Emergency Physicians [1]. The overall result of overcrowding, at its most fundamental level, is that the length of holding admitted patients within the ED when there are no inpatient beds available, known as "boarding," is extended, which in turn increases negative patient outcomes [2,3].

ing waveguide or "multibox" structure with a 15-fold greater sensitivity than silicon ring resonators with a "traditional" geometry [71,72]. However, the limit of detection for these devices suffers from lower Q-factors, or broadening of the resonance peak. Furthermore, the small feature size of the "multibox" structures requires e-beam lithography to fabricate, so these designs do not scale well for manufacturing.

It has been hypothesized that spiral "ring" resonators would increase the surface area available for sensing, while maintaining a compact footprint. Xu et al. developed a spiral cavity resonator and used it to monitor the kinetics of biotin–streptavidin binding [73]. By lengthening the cavity, they relaxed the critical coupling conditions and made the spiral resonator less sensitive to fabrication variations. The effective interaction length of 1.27 mm was fit into a 110 by 110 μm footprint, while still achieving a respectable Q-factor of 20,000. Streptavidin binding to biotin at concentrations as low as 1.7 nM was demonstrated.

Other groups have pursued the Vernier effect to enhance ring resonator sensitivity and free-spectral range by cascading multiple ring resonators in-serial between two bus waveguides [74–76]. Liu et al. have described a ring resonator biosensor based on three cascaded rings that would yield both high sensitivity and a wide range of operation [77]. However, this configuration's practicality for commercialization is diminished by fabrication variations, which make it difficult for three coupled ring resonators to share a resonant wavelength as designed. Many other resonant biosensor structures have also been described, including toroids, beads, and fibers [78,79].

Beyond physical enhancements to ring sensitivity, a critical threshold to commercialization of integrated photonic sensors at the point-of-care is the integration with microfluidics for sample delivery. One approach to ring resonator biosensor packaging was described by Laplatine et al. in 2018 [80]. Here, a "fan-out" approach was employed to reduce the amount of silicon used (limiting it to just the area of the rings themselves, along with germanium photodiodes) as a way to limit per-chip cost, while providing enough surface area for microfluidic and electronic packaging (Fig. 8.13); an outstanding demonstration of packaging for an active device. Even simpler and lower-cost approaches are desirable.

To further simplify and reduce the cost of ring resonator-based biosensors for diagnostics, Cognetti et al. developed a method for integrating sensor chips with passive microfluidics, and demonstrated the use of microring resonators for the detection of antibodies against SARS-CoV-2 in human samples [81]. Because the plastic micropillar microfluidic card transports fluids being analyzed via capillary flow, no pumps or power are required. Use of a grain of rice-sized photonic sensor chip also reduces the per-assay cost. An optical hub was codeveloped with the disposable to allow grating coupled light input/output and rapid alignment (Fig. 8.14).

8.4.5   Waveguide-enhanced Raman spectroscopy (WERS)

The photonic sensors discussed thus far perform well for the detection of "large" molecules, such as proteins and oligonucleotides, but their reliance on localized changes in refractive index makes them less useful for the detection of small molecule analytes. As an alternative to photonic sensing methods reliant on changes in lo-
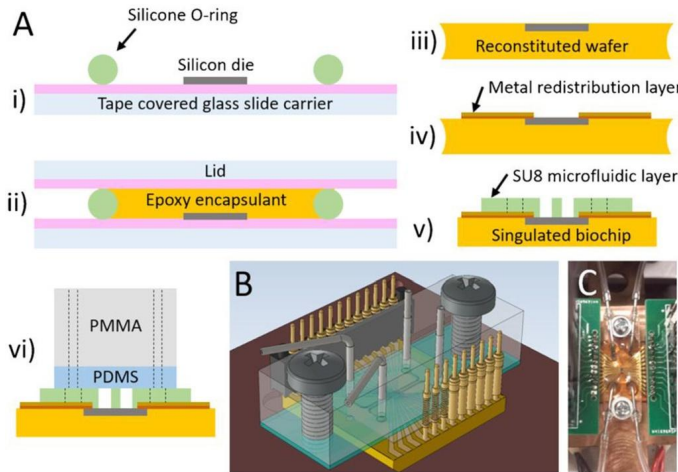
Figure 8.13 Packaging ring resonator biosensors using a lab-scale fan-out process. Panel (a) shows the steps in the process from individual sensor die resting on a tape-covered glass slide carrier to the final epoxy-packaged chip with polymer (SU-8), PDMS, and PMMA microfluidic microchannel. (b) Overall schematic of electrical and microfluidic connections. (c) Photograph of the final device. Reprinted from reference [80], Copyright (2018), with permission from Elsevier.

cal refractive index, waveguide-enhanced Raman spectroscopy (WERS) enables the detection of molecules based on their infrared spectroscopic signature [82,83]. This enables direct detection of targets of interest without recourse to immobilized capture molecules, such as antibodies or nucleic acids. Analyte concentration with concomitant spectral simplification may be accomplished in WERS via the use of sorbent films (Fig. 8.15). Though such sorbents have primarily found use in detection of gas-phase analytes [84], in principle such materials could also be used to enhance detection of analytes in biofluids. Miniaturized instrumentation for Raman spectroscopy is available from several manufacturers. Thus while at an early stage, we can anticipate that advances in this area will enable its use at PoC.

8.4.6 Integration of light sources

Although most resonant optical biosensing work has used expensive bench-top tunable laser sources and detectors, there is considerable interest in adapting CMOS-compatible processes for monolithic integration of a laser, transducer, and detector into a single chip. Several groups have demonstrated various approaches toward this goal. Moock et al. described a novel approach for tuning an inexpensive fixed-wavelength laser to interrogate the resonance of ring resonator arrays [85]. The incorporation of triangular SOI ring resonator into the cavity enabled them to isolate a directional coupler, heating electrode, and sensing trench to each side of the resonator. Their method of time-division multiplexing used a fixed-wavelength source at 1550 nm and a modulated voltage applied to the ring heater electrodes to sweep

Endomicroscopy

<div style="text-align:right">

9

</div>

Stamatia Giannarou, Chi Xu, and Alfie Roddan
Hamlyn Centre for Robotic Surgery, Department of Surgery and Cancer, Imperial College London, London, United Kingdom

9.1 Technology

The main goal of surgical oncology is to achieve complete resection of cancerous tissue with minimal iatrogenic injury to surrounding tissue. In practice, this often presents a formidable challenge to surgeons. This is because it is difficult to distinguish tumor tissue from surrounding healthy tissue, especially when approaching tumor margins. There is evidence that increasing the extent of tumor resection substantially improves overall and progression-free survival in oncological surgery. However, this requires visualization of the tissue at a cellular level. Histopathological analysis still remains the gold-standard for differential diagnosis, but it has significant limitations intraoperatively, such as tissue sampling errors, interruption of the surgical workflow, and lack of interaction with pathologists to optimize the selection of the biopsy sample.

Endomicroscopy is an emerging imaging modality, which enables in vivo and in situ visualization of the tissue at microscopic level. Recent pilot studies suggest that this technique may have a role in identifying pathological tissue and improving tumor resection rates predominantly in neurosurgery and in the gastrointestinal, urological, and the respiratory tracts. To date, several endomicroscopic imaging systems, based on different fundamental optical imaging technologies, have been commercialized for clinical use.

The NVisionVLE platform (NinePoint Medical, USA) was a volumetric laser endomicroscopy (VLE) imaging system, which could create in real-time a sequence of two-dimensional cross-sections, enabling the visualization of tissue microstructures. This system uses advanced optical coherence tomography (OCT) to capture images up to 3 mm beneath the tissue surface at a 7 micron resolution, delivering up to 25 times higher resolution than endoscopic ultrasound.

Another endomicroscopic imaging system is the Endocyto (Olympus Medical Systems, Japan). This is a flexible, contact endoscope with magnification of up to 520x, which enables real-time in vivo observation of cells and nuclei, assisting tissue characterization at microscopic scale during endoscopic examinations. To observe the cellular morphology of the superficial mucosal layer, the tissue is stained and the objective lens of the endocytoscope is brought into contact with the mucosa. Imaging of the cellular structures is achieved via light scattering. This imaging system has been incorporated by Olympus into gastroscopic and colonoscopic platforms for in vivo and in situ lesion assessment, which can facilitate decision-making and allow therapeutic intervention. Similar, non-commercial systems include a fiber bundle endocytoscope,

visualize tissue microstructure in situ at the cellular level provides clinicians with invaluable information for diagnosing diseases and assessing treatment efficacy [27]. However, despite its significant advantages, pCLE image quality remains inherently limited by the design of its hardware, which relies on an optical fiber bundle. These bundles consist of tens of thousands of irregularly arranged fibers, each acting as a single-pixel detector, resulting in images with artifacts, noise, low contrast, and limited resolution [37–39]. This has led to a growing interest in the development and application of super-resolution (SR) techniques to enhance the quality and resolution of pCLE images. This section aims to provide a comprehensive overview of SR methods applied to pCLE, with a particular focus on deep learning-based approaches.

Super-resolution (SR) techniques have demonstrated significant potential in enhancing the image quality of pCLE images [40]. In the context of pCLE, multiframe image super-resolution (MISR) [20] approaches capitalize on multiple low-resolution (LR) pCLE images taken at slightly shifted field-of-views, fusing them into a single high-resolution (HR) image to augment spatial information and unveil previously obscured details. Though MISR can potentially provide superior image quality, it necessitates precise registration of LR images, which can be computationally demanding and challenging for real-time applications. Alternatively, single-image super-resolution (SISR) employs signal processing techniques to produce HR pCLE images with enhanced details, making it more suitable for real-time purposes compared to MISR. A notable approach to SISR is exemplar-based super-resolution (EBSR), which utilizes encoder-decoder deep learning architectures to generate HR images by learning the correspondence between LR and HR images.

SR dataset generation: To train the EBSR framework, pairs of low-resolution (LR) and high-resolution (HR) images are required. Owing to the limited availability of ground truth HR pCLE images, a registration-based mosaicking method [20] is utilized to create HR images. Mosaicking acts as a conventional SR technique, merging several registered input frames by averaging their temporal data. The produced mosaics serve as a source of HR pCLE images. However, since mosaicking generates a single expansive field-of-view mosaic image from multiple input LR images, it does not directly supply a corresponding HR image for each LR input. To address this issue, the mosaic-to-image diffeomorphic spatial transformation derived from the mosaicking process is employed to distribute and trim the combined information from the mosaic back into each input LR image space. These trimmed images are treated as the ground truth HR pCLE images for EBSR training. Furthermore, to create LR images that align perfectly with HR images, the fiber positions of HR images and a combination of additive and multiplicative Gaussian noise are leveraged to produce well-aligned LR images.

Deep learning for SR: After generating the SR dataset for pCLE, the deep learning training framework is also crucial. In this section, two training frameworks for the pCLE SR task are introduced:

- Adversarial training with cycle consistency (ATTC): The framework [38] uses an adversarial network, which consists of two separate models: a SR network, which learns to improve the resolution of the images, and a discriminative network, which
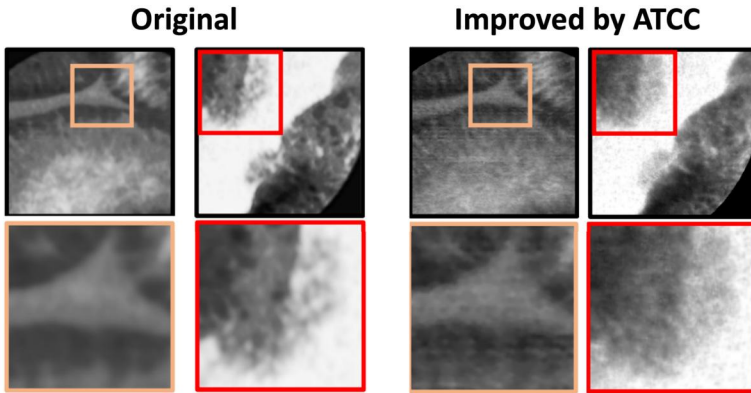
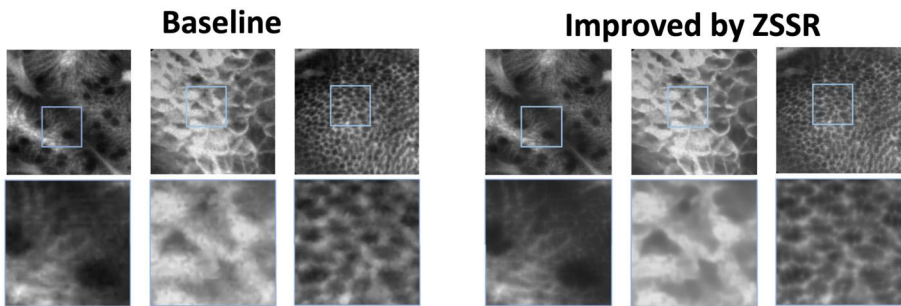**Figure 9.2** The super-resolution of pCLE improved by ATTC [38].

Figure 9.3 The super-resolution of pCLE improved by ZSSR [39].

tries to distinguish images generated by the SR network from the real HR images. The goal is for the SR network to learn to fool the discriminative network, ultimately leading to the generation of super-resolved images. A cycle consistency block is added to the adversarial training to impose a consistency between the HR images and the initial LR images. This is achieved by constraining the super-resolved image to have similar physical acquisition properties to the initial LR image. The results improved by ATTC are shown in Fig. 9.2.

- Zero-shot super-resolution (ZSSR): ZSSR techniques have garnered interest due to their self-supervised nature and independence from ground-truth HR images. ZSSR pipelines can be tailored for pCLE images by introducing physically motivated downsampling kernels, which account for the endomicroscope's irregular fiber-based sampling pattern and realistic noise patterns. By exploiting the structure of pCLE videos, this approach can further improve the quality of reconstructed HR images, showing superior performance in image quality when compared to baseline methods [39]. The results improved by ZSSR are shown in Fig. 9.3.

Deep learning-based SR methods have significantly advanced the quality of pCLE images, enhancing their diagnostic potential and clinical interpretability. The meth-

Optical coherence tomography technology in clinical applications

10

Jack C. Tang[a], Regina Magalhães[a], Anna Wisniowiecki[a,b], Diego Razura[a,c], Clayton Walker[a,b], and Brian E. Applegate[a,d,e]

[a]Caruso Department of Otolaryngology – Head & Neck Surgery, Keck School of Medicine, University of Southern California, Los Angeles, CA, United States, [b]Department of Biomedical Engineering, Texas A&M University, College Station, TX, United States, [c]James H. Quillen College of Medicine, Eastern Tennessee University, Johnson City, TN, United States, [d]Department of Ophthalmology, Keck School of Medicine, University of Southern California, Los Angeles, CA, United States, [e]Alfred E. Mann Department of Biomedical Engineering, Viterbi School of Engineering, University of Southern California, Los Angeles, CA, United States

10.1   Introduction

Humphrey Zeiss (now Carl Zeiss Meditec AG) introduced the first commercial optical coherence tomography (OCT) system for retinal imaging in 1996 [1]. This initial commercial offering followed rapid development based on research in the late 1980s and early 1990s [2–4]. The brisk translation from research to clinical tool attests to the clear clinical need filled by OCT in ophthalmic imaging. It offered high-resolution cross-sectional images through the entire thickness of the retina without contacting the eye. In the intervening years, various incarnations of OCT have been developed into clinical devices for imaging the anterior segment of the eye [5], coronary [6], and peripheral artery disease [7], Barrett's esophagus [8], and ear infections [9]. Commercialized clinical systems have been developed for many medical specialties, including ophthalmology, cardiovascular, oncology, dermatology, and dental [10,11]. New preclinical prototype systems are being developed for these fields and more, which we will discuss in the second half of this chapter [12–17].

In this chapter, we first introduce the essential theoretical background needed to understand how OCT images are formed, as well as the underlying contrast mechanisms of functional extensions of OCT. We then discuss a selection of clinical and pre-clinical applications of OCT, which we hope will illustrate the vast and diverse impact that OCT has on many medical specialties.

10.2   Theoretical background

Small changes in tissue refractive index result in backscattering of incident light. This scattering signal is fundamentally what OCT measures. In an OCT imaging system, the sample of interest is illuminated with a coherent light source. Light is reflected at
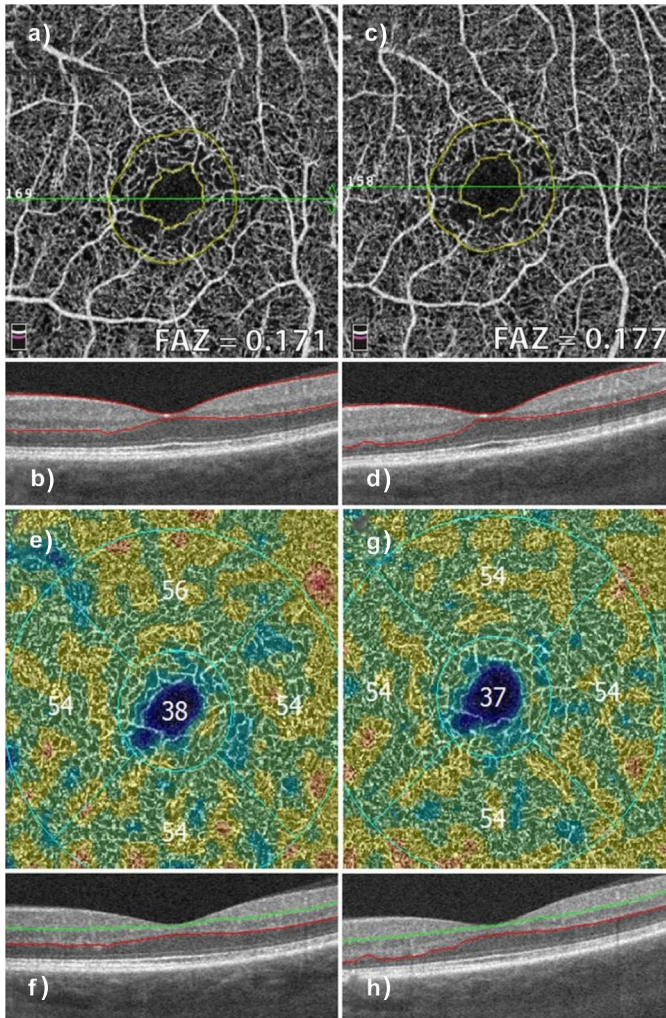
Figure 10.4 OCT monitoring of diabetic retinopathy (DR). Foveal avascular zone (FAZ) area and vessel density measurements. Example of a patient with severe non-proliferative diabetic retinopathy. Images in the left column were taken 12 months prior to images in the right column. a), c) Superficial retinal slab projection showing automated FAZ area measurements. Note parafoveal capillary drop out and slight increase in FAZ area over time. b), d) B-scan showing corresponding segmentation boundaries. e), g) Vessel density map of the deep retinal slab for the same patient and timepoints. Note slight drop in vessel density in the superior quadrant. f), h) B-scan with corresponding segmentation lines. Figure is reprinted from [60] with permission from Nadia K. Waheed, MD, MPH and is licensed under CC BY 4.0 (https://creativecommons.org/licenses/by/4.0/).

Innovations in signal/image processing and data analysis in optical microscopy

11

Lucas Kreiss[a,b], Kevin C. Zhou[a,c], Clare B. Cook[a], Shiqi Xu[a], Amey Chaware[a], and Roarke Horstmeyer[a,d]

[a]Department of Biomedical Engineering, Duke University, Durham, NC, United States, [b]Institute of Medical Biotechnology, Friedrich-Alexander University (FAU), Erlangen, Germany, [c]Department of Electrical Engineering & Computer Sciences, University of California, Berkeley, CA, United States, [d]Department of Electrical and Computer Engineering, Duke University, Durham, NC, United States

11.1 Introduction

The field of biophotonics in general, and optical microscopy in particular, heavily relies on signal processing and data analysis to extract or distill information and ultimately improve our understanding of the sample under interrogation. Besides the fundamental imaging physics or the biological properties that are exploited for imaging, these emerging computational methods are essential to all imaging modalities. In this chapter, we present an overview of well-established and current state-of-the-art methods, and their representative applications sampled across this broad field. Furthermore, we also discuss current challenges and limitations, including ethics, interpretability, and privacy issues for datasets and AI tools.

Although biological image data can simply be regarded as N-dimensional datapoints, where N is the number of pixels or voxels in the image, several key properties deserve special mention, which distinguish biological image data from more general forms of data, and even imaging data from other fields.

- **What's so special about images?** An image is a specific type of data, spatially organized into an typically 2- or 3-dimensional array. What distinguishes an image from an unordered data structure with the same dimensionality (i.e., same number of entries as pixels) is that neighboring entries have a tendency to be unconditionally similar, rendering useful the concept of "locality" and "cropping."
- **Resolution:** The resolution of an image is basically the smallest level of detail that an image covers. Depending on the implementation, the image resolution can be limited optically (see diffraction limit below) or limited by sampling (e.g., the available pixel size on the sensor). There are many possible definitions of resolution, such as the Abbé limit, the two-point criterion, the Sparrow criterion, or the Rayleigh criterion.
- **Field-of-view (FOV)** is the area that can be imaged by a microscope in a single exposure.

- **Space-bandwidth product (SBP)** is a measure for the information capacity of an optical system. This SBP is typically limited for a given system and results from a fundamental trade-off between resolution and FOV.
- **Contrast mechanism:** the fundamental process in which light interacts with a sample, and which gives rises to the imaging signal. Simple white-light microscopy, for instance, uses scattering and absorption properties of samples; phase microscopy techniques measure phase contrast based on refractive index (RI) differences, whereas other imaging modalities use intensity or fluorescence intensity or lifetime of fluorescence.
- **Signal-to-noise ratio (SNR):** as the name suggests, the SNR is the ratio between what is defined as signal (see contrast mechanisms above) to the unwanted background noise (see Section 11.2 below).

As such, many image processing and data analysis techniques focus on improving one or multiple of these properties, with the ultimate goal of extracting new knowledge about the sample under study.

In the following sections, we will present well-established and state-of-the-art methods that can improve images via at least one of the criteria. Furthermore, we show examples of data analysis that can be used to exploit the information content of images for automated decision-making, based on machine learning. Most of these tools can be used post-hoc, e.g., for improving image quality, suppress artifacts or extract meaningful and quantifiable information. However, some other techniques rely on in-built computation to reconstruct images in the first place. Therefore we will make our way starting at denoising and resolution enhancement in Sections 11.2 and 11.3, respectively. Methods of image stitching and registration to enhance FOV and SBP of images are shown in Section 11.4. Section 11.5 then targets "qualitative image enhancement" as a stepping stone to quantitative extraction of image information in Section 11.6. Finally, we discuss ethics in Section 11.7 and end with a summarizing conclusion.

11.2 Denoising
11.2.1 What is noise?

Due to the stochastic nature of photon arrival times and associated fluctuations in the intensity of light, the imperfect readout, and electronics, the measured image is usually corrupted by noise. This noise is widely modeled as an additive white Gaussian (AWG) noise,

$$g(x, y) = f(x, y) + n(x, y), \tag{11.1}$$

where f is the original clean image; g is the measured noisy image; x, y are the spatial coordinates, and n is white Gaussian noise with standard derivation σ. In practice, σ is usually measured *a priori*, or estimated by analyzing a flat region on the image. During the last three decades, a high number of denoising techniques have been developed. This section is organized as follows: Section 11.2.2 discusses spatial filtering
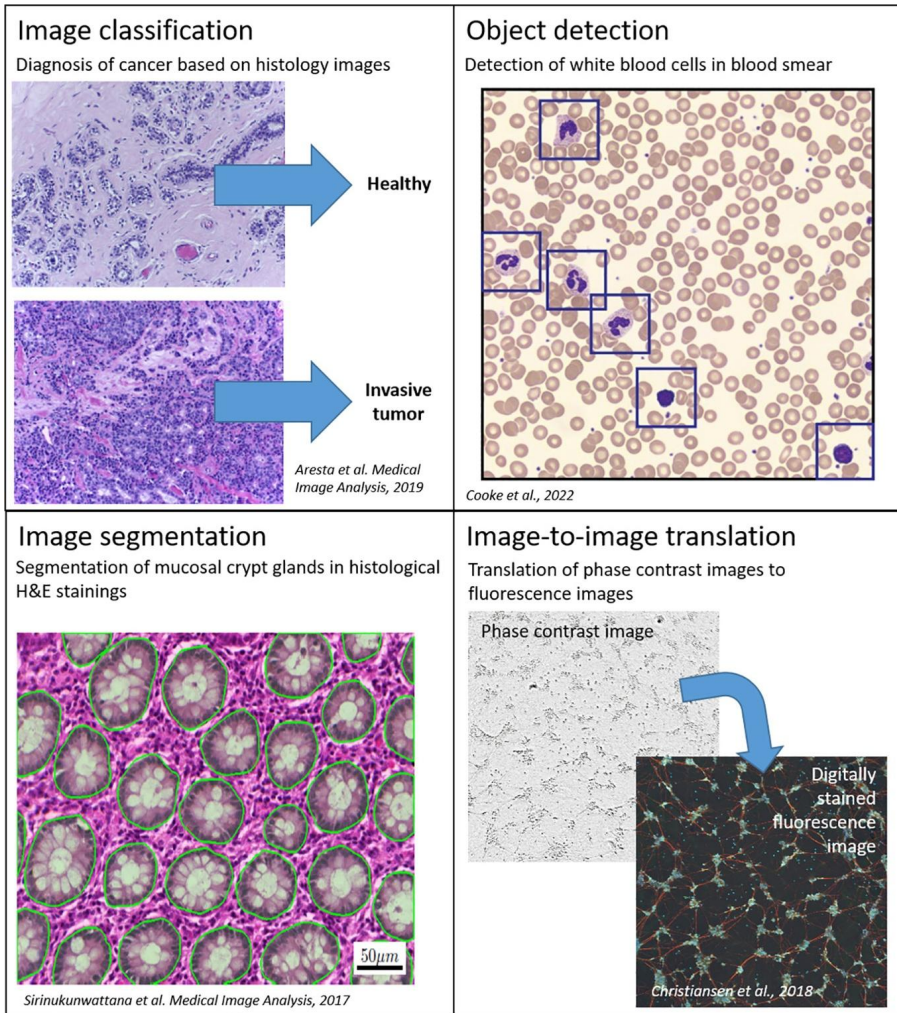
Figure 11.3 The four cases of image classification, object detection, segmentation, and image-to-image translation for different examples. A) Image classification for the example of tumor classification in H&E histology images of breast tissue (adapted from [103], licensed under CC-BY-NC-ND 4.0 ©2018, Copyright Elsevier). B) Object detection for the example of detecting white blood cells in blood smears of COVID patients (adapted from [101], licensed under CC-BY-NC-ND 4.0 ©2022). C) Image segmentation for the example of segmenting mucosal crypt glands in H&E histology images of colon tissue (adapted from [104], © 2016 Elsevier B.V. with permission from Elsevier and Copyright Clearance Center). D) Image-to-image regression for the example for predicting artificial fluorescent markers from phase microscopy images (adapted from [105], under Elsevier user license with permission from Elsevier and Copyright Clearance Center).

Recent innovations in signal and image processing and data analysis in Raman spectroscopy

Oleg Ryabchykov[a,b], Dana Cialla-May[a,b], Anja Silge[a,b], Sara Mostafapour[a,b], Azadeh Mokari[a,b], Ruihao Luo[a,b], Pegah Dehbozorgi[a,b], Jhonatan Contreras[a,b], Jürgen Popp[a,b], and Thomas Bocklitz[a,b,c]

[a]Leibniz Institute of Photonic Technology, Member of Leibniz Health Technologies, Member of the Leibniz Centre for Photonics in Infection Research (LPI), Jena, Germany, [b]Institute of Physical Chemistry (IPC) and Abbe Center of Photonics (ACP), Friedrich Schiller University Jena, Member of the Leibniz Centre for Photonics in Infection Research (LPI), Jena, Germany, [c]Work group Artificial Intelligence in Spectroscopy and Microscopy, University of Bayreuth, Bayreuth, Germany

12.1 Introduction

Raman spectroscopy is a type of vibrational spectroscopy, which is based on the inelastic scattering of light by the sample. The energy of Stokes and anti-Stokes scattered light is slightly shifted due to the interaction with molecular vibrations, thus such shifts reveal the vibrational energy levels of the investigated molecules (see Chapter 4 in this volume and Fig. 12.1A).

The Raman effect was discovered and interpreted in 1928 [1], but its usage in the biomedical fields only emerged in recent decades due a few technical obstacles, which made the implementation of Raman spectroscopy difficult and cost ineffective. Major advances that were necessary for the implementation of Raman instruments were related to the development of the laser and confocal scanning microscopy in the 1950s
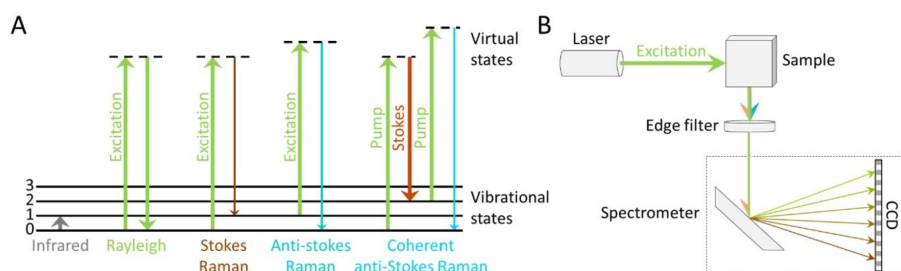

Figure 12.1 Principles of Raman spectroscopy. The energy diagram (A) demonstrates infrared absorption energy, Rayleigh scattering process, Stokes Raman scattering, anti-Stokes Raman scattering, and CARS processes. The simplified sketch of a Stokes Raman measurement system (B) demonstrates necessary components for a typical Raman spectroscopic instrument.

AI-driven innovations in signal/image processing and data analysis for optical coherence tomography in clinical applications

Danuta M. Sampson[a,b] and David D. Sampson[c]
[a]Lions Eye Institute, Nedlands, WA, Australia, [b]The University of Western Australia, The School of Allied Health, Optometry Division, Perth, WA, Australia, [c]School of Computer Science and Electronic Engineering, The University of Surrey, Guildford, United Kingdom

Chapter highlights

- Optical coherence tomography (OCT) is a game changer in ophthalmic care.
- OCT is growing beyond ophthalmology, impacting other medical fields, including cardiology, gastroenterology, dermatology, otolaryngology, dentistry, and pulmonary, cancer, and reproductive medicine.
- The advancement of signal and image processing and data analysis methods is a crucial part of OCT's growth.
- There is a recent shift in OCT signal/image analysis methods towards AI, especially deep-learning methods.
- The clinical utility of AI-OCT systems is still limited due to the small size of the datasets, varying standards and regulations between OCT device manufacturers, institutions and countries, the limited number of standardized and sharable datasets and data analysis methods, and ethical issues of bias and privacy.

Preface

Optical coherence tomography (OCT) is an imaging technique that enables rapid, noninvasive acquisition of near-cellular-scale resolution, structural cross-sectional and volumetric images of scattering objects, such as human tissues [1–3]. OCT can also be extended by hardware and software modification to provide alternative tissue contrast and additional information. For example, OCT angiography (OCTA) enables the visualization of vessels [4], and OCT elastography (OCE) probes the mechanical properties of tissues [5]. Polarization-sensitive OCT enables visualization of the birefringence properties of tissue, related to its structure and order [6].

validated generative adversarial networks to enhance the resolution, but they struggled to reproduce realistic speckle noise [28,29]. Yuan et al. built pixel-level registered pairs of *en face* low-resolution and high-resolution OCT images based on experimental data and introduced the receptive field block into the generative adversarial networks to learn the complex mapping relationship between low- and high-resolution image pairs [109]. It was demonstrated through imaging of phantom and biological samples that the lateral resolutions were improved at greater imaging depths.

MAS OCT, as mentioned above, has been extended to MAS-Net OCT, a deep-learning-based multiple aperture synthetic method [110]. This technique required first modifying the MAS OCT instrument based on the concept introduced by Bo et al. [107] to be able to collect low- and high-resolution OCT B-scans. Pairs of low-and denoised high-resolution images are fed into the developed MAS-Net, a GAN constructed from U-Net with residual dense blocks (RDBs) and a multiscale discriminator. The authors showed that the MAS-Net OCT method has the intriguing potential to improve transverse resolution and optimize depth of focus. For example, the authors showed that the MAS-Net could sharpen/reduce the width of the structure by a factor of two compared to the original images.

13.3   OCT image segmentation

Segmentation, e.g., labeling of pixels in structural OCT B-scans according to morphology, is a critical component of quantitative analysis, and therefore we devote a good deal of space to considering it in this chapter. The accurate boundary detection of tissue layers in cross-sectional OCT images and segmentation of characteristic features, e.g., drusen and cysts, which appear in the retina due to age-related macular degeneration, and border detection in skin tumors, are vitally important aspects of clinical diagnosis using OCT. Segmentation can be challenging, first and foremost, because the ever-present speckle may obscure tissue layer boundaries and other morphological features [70]. In addition, it can be challenging due to the inhomogeneity of the optical contrast within the image. For example, contrast decreases with depth due to scattering and absorption in tissue [111]. Contrast can be locally lower due to the presence of image artifacts [112] or blood vessels or surface structures that generate shadows, masking the structures below. Then, the very presence of pathology, which is the most interesting aspect for healthcare professionals, makes the segmentation a more challenging task. There is a huge number of pathologies, and they have different footprints in OCT images. Fig. 13.5 shows B-scans of healthy and diseased retinas to help the reader better understand how retinal B-scans can vary according to pathology.

Manual segmentation is the gold standard for OCT images. It requires outlining structures slice-by-slice, and is thus expensive, tedious, and subject to human error. Furthermore, as discussed in Section 13.1.3, the widespread availability of OCT in ophthalmology and an increase in the number of patients with retinal diseases make it impossible to match the availability of expert humans with the number of scans. Therefore there is a need for automated segmentation methods to provide accuracy close to that of expert raters with high consistency. This section discusses the most recently introduced methods for OCT image segmentation.
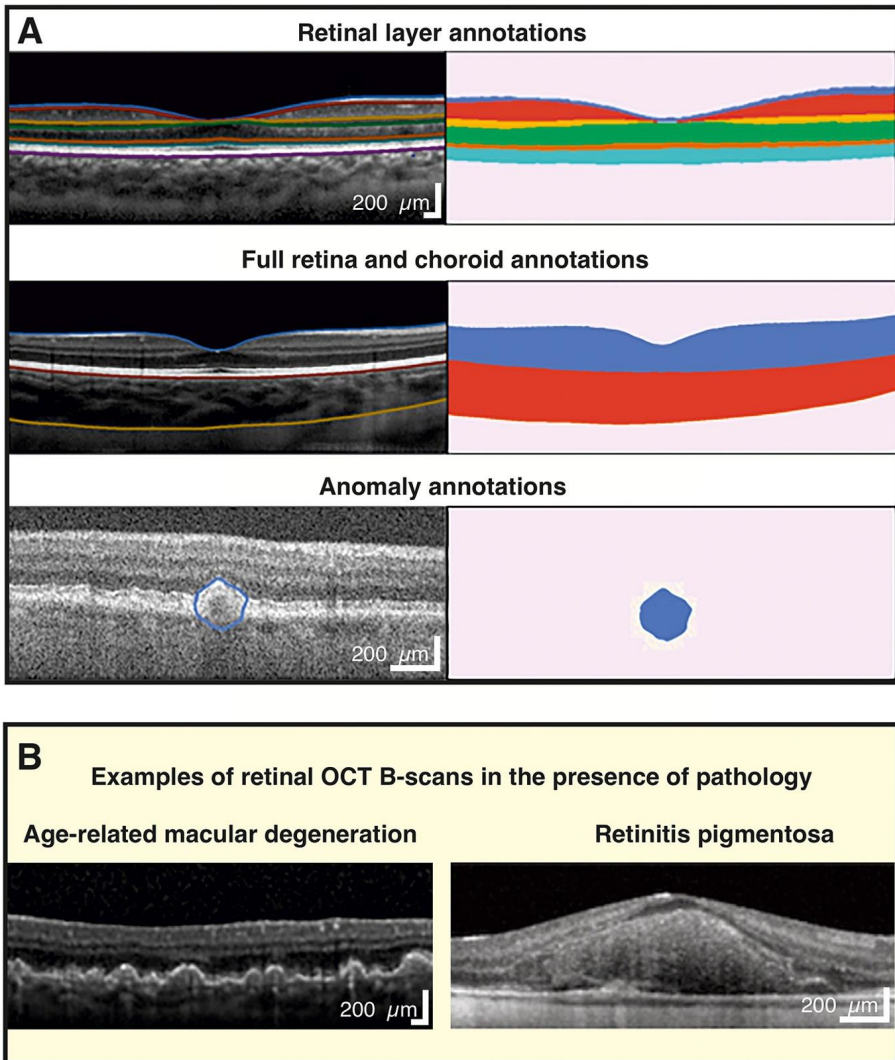
Figure 13.5 A) Examples of annotated OCT images showing the manually annotated boundaries generated by an expert (left) and by a computational model (right). B) Examples of retinal images with pathologies. Image size approx. 6 × 0.7 mm. Panel A was adapted from [113] with permission from Elsevier. The Age-related macular degeneration image is from Duke DME/AMD publicly available dataset [114]. Panel B was adapted from [115] with permission from Elsevier.

13.3.1   Retinal layer segmentation

Retinal disease can affect as little as a single layer of this multilayered tissue. Therefore the segmentation of retinal layers to measure and map layer thickness and reflectivity is a critical task, not least towards identifying sensitive biomarkers of disease